BIOCHEMISTRY
including biophysical chemistry & molecular biology

Article

pubs.acs.org/biochemistry

Cofactor Binding Triggers a Molecular Switch To Allosterically Activate Human UDP-α-D-glucose 6-Dehydrogenase

Nicholas C. Sennett, Renuka Kadirvelraj, and Zachary A. Wood*

Department of Biochemistry and Molecular Biology, University of Georgia, Athens, Georgia 30602, United States

ABSTRACT: Human UDP-α-D-glucose dehydrogenase (hUGDH) catalyzes the NAD^+-dependent oxidation of UDP-α-D-glucose (UDG) to produce UDP-α-D-glucuronic acid. The oligomeric structure of hUGDH is dynamic and can form two distinct hexameric complexes in solution. The active form of hUGDH consists of dimers that undergo a concentration-dependent association to form a hexamer with 32 symmetry. In the presence of the allosteric feedback inhibitor UDP-α-D-xylose (UDX), hUGDH changes shape to form an inactive, horseshoe-shaped complex. Previous studies have identified the UDX-induced allosteric mechanism that changes the hexameric structure to inhibit the enzyme. Here, we investigate the role of the 32 symmetry hexamer in the catalytic cycle. We engineered a stable hUGDH dimer by introducing a charge-switch substitution (K94E) in the hexamer-building interface ($hUGDH_{K94E}$). The k_{cat} of $hUGDH_{K94E}$ is ~160-fold lower than that of the wild-type enzyme, suggesting that the hexamer is the catalytically relevant state. We also show that cofactor binding triggers the formation of the 32 symmetry hexamer, but UDG is needed for the stability of the complex. The $hUGDH_{K94E}$ crystal structure at 2.08 Å resolution identifies $loop_{88-110}$ as the cofactor-responsive allosteric switch that drives hexamer formation; $loop_{88-110}$ directly links cofactor binding to the stability of the hexamer-building interface. In the interface, $loop_{88-110}$ packs against the Thr131-loop/α6 helix, the allosteric switch that responds to the feedback inhibitor UDX. We also identify a structural element (the S-loop) that explains the indirect stabilization of the hexamer by substrate and supports a sequential, ordered binding of the substrate and cofactor. These observations support a model in which (i) UDG binds to the dimer and stabilizes the S-loop to promote cofactor binding and (ii) cofactor binding orders $loop_{88-110}$ to induce formation of the catalytically active hexamer.

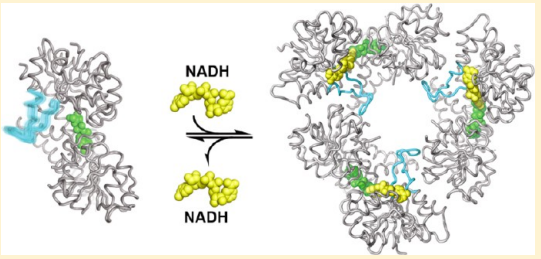

Human UDP-α-D-glucose 6-dehydrogenase (hUGDH) catalyzes the NAD^+-dependent oxidation of UDP-α-D-glucose (UDG) to produce UDP-α-D-glucuronic acid (UGA).[1] The product of hUGDH is the essential substrate in glucuronidation, an important pathway in the phase II metabolism of toxins and drugs.[2] The covalent attachment of glucuronic acid to xenobiotics produces glucuronides that are rapidly excreted through the biliary tract or kidneys. In some cancers, glucuronidation has been shown to act as a drug resistance mechanism by enhancing the clearance of potentially beneficial chemotherapeutics.[3−7] It may be possible to sensitize these drug resistant tumors to existing chemo-therapeutics by inhibiting hUGDH. Understanding how hUGDH is regulated may help us achieve this goal.

hUGDH has a dynamic structure and can associate to form two distinct hexameric complexes.[8−10] Most crystal structures of hUGDH reveal a hexamer with 32 symmetry, believed to represent the active conformation of the enzyme (Figure 1A).[8,10,11] We have previously described how the feedback inhibitor UDP-α-D-xylose (UDX) converts the 32 symmetry hexamer to an inactive, horseshoe-shaped complex (Figure 1A).[8,9] The plasticity of the oligomer is due to the flexibility of the NAD^+ binding (NB) domain and nucleotide−sugar binding (SB) domain (Figure 1A).[9] The NB and SB domains have complementary surfaces that allow three dimers to associate into the different hexameric complexes. The hexamer-building (HB) interface formed between the dimers is remarkable for its conformational flexibility; the domains of adjacent dimers can rotate in a concerted fashion while maintaining contact with the HB interface (Figure 1B).[9] The rotation of the domains allows the enzyme to bind the substrate and release products during the catalytic cycle.[9,10]

Because of the flexibility of the HB interface, the hexamer is a relatively unstable complex that readily dissociates into a concentration-dependent mixture of dimers, tetramers, and hexamers.[8,9] Here, we address the factors that stabilize the 32 symmetry hexamer and the role it plays in the catalytic cycle. Using a stable hUGDH dimer, we show that the ordered binding of UDG and cofactor triggers the formation of the 32 symmetry hexamer and that the hexamer is the relevant catalytic state. The structure of the hUGDH dimer identifies the cofactor sensitive allosteric switch and a mechanism by which substrate can stabilize the hexamer. Finally, we present a structurally detailed catalytic cycle that incorporates the flexible HB interface and the feedback inhibition mechanism.

Received: August 8, 2012
Revised: October 17, 2012
Published: October 29, 2012

dx.doi.org/10.1021/bi301067w | *Biochemistry* 2012, 51, 9364−9374

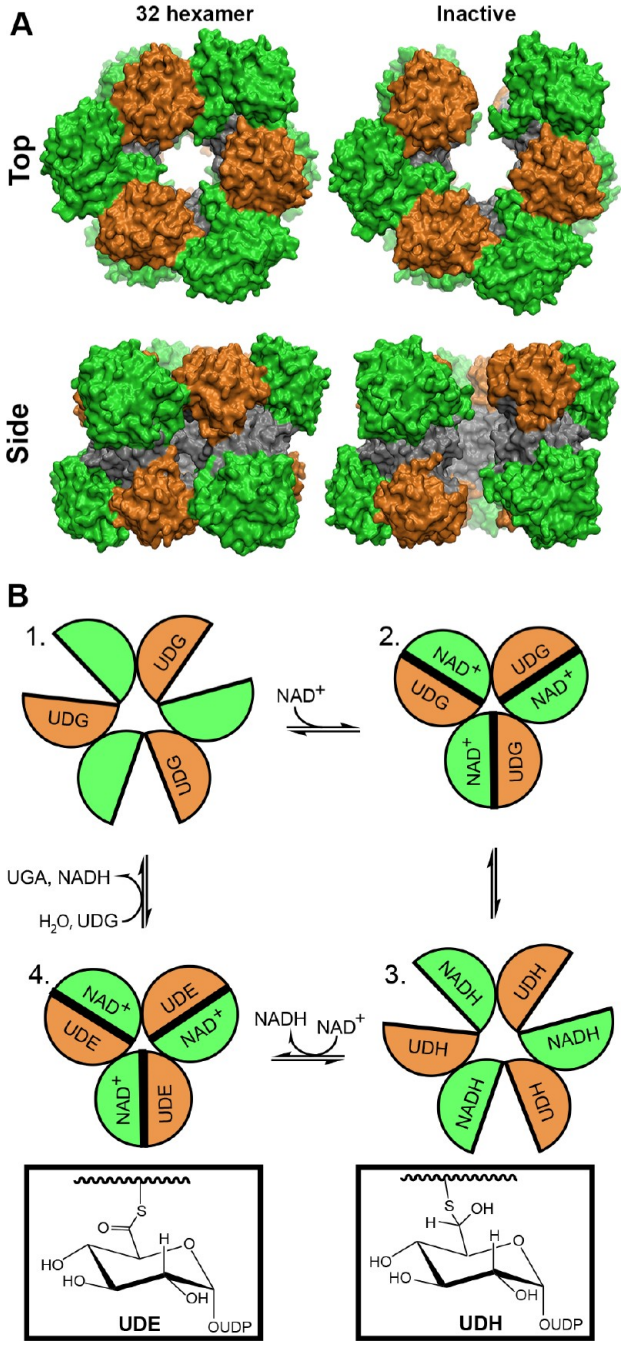

Figure 1. Catalytic cycle and regulation of hUGDH. (A) Top and side views of the 32 symmetry hexamer [left, Protein Data Bank (PDB) entry 2Q3E] and the inactive, UDX-bound hexamer (right, PDB entry 3PTZ) showing the NB (green), SB (orange), and dimerization (gray) domains. (B) Cartoon showing that the NB and SB domains rotate to facilitate the binding of substrates and release of products during the catalytic cycle. For the sake of clarity, only the top trimer of hUDGH is shown with the NB and SB domains depicted as semicircles and colored as described above. (1) The catalytic cycle of hUGDH begins with UDG binding to the open domain conformation. (2) NAD^+ binds, and the NB and SB domains close. (3) NAD^+ oxidizes UDG to an aldehyde, which is attacked by Cys276, which forms UDP-α-D-6-thio-glucose (UDH). The domains rotate open, and NADH is exchanged for NAD^+. (4) The domains then close, and UDH is oxidized to UDP-α-D-6-thio-gluco-hexodialdo-1,5-pyranose (UDE). Finally, UDE is hydrolyzed to release UDP-glucuronic acid (UGA). The chemical structures of the covalent UDH and UDE intermediates are illustrated in the boxes below the cartoon.

MATERIALS AND METHODS

Crystallization, Data Collection, and Refinement. The $hUGDH_{K94E}$ construct was expressed and purified by the same procedure that was previously used for the wild-type enzyme.[8] Crystals were grown at 25 °C by sitting drop vapor diffusion with 1 μL of 10 mg/mL $hUGDH_{K94E}$ with 5 mM UDG and 1 μL of well solution [200 mM $MgCl_2$, 100 mM citrate buffer (pH 5.0), and 10% PEG 20000]. Bipyramidal crystals appeared in 2−3 weeks. For cryoprotection, the crystals were soaked incrementally in the well solution containing 5, 10, 15, and 20% glycerol and then plunged into liquid nitrogen. Data were collected on the SERCAT 22-ID beamline at APS with at wavelength of 1 Å (180° with a 1° oscillation and a 1 s exposure) using a MAR300 CCD detector. The images were processed in space group $P2_1$ using XDS.[12] Data collection statistics are listed in Table 1. The program Xtriage from the Phenix software suite[13] detected pseudomerihedral twinning related by an *l*, −*k*, *h* operator. The Britton plot estimates a maximal twin fraction of 32%. The structure was determined using a single peptide chain of hUGDH, UDG, and NADH [Protein Data Bank (PDB) entry 2Q3E] as a search model in MOLREP.[14] The molecular replacement solution was subjected to rigid body refinement followed by manual rebuilding in Coot.[15] Phenix.refine was used for positional refinement and automatic detwinning.[13] During the transfer to Phenix, the R_{free} set was corrupted. We calculated a posterior R_{free} by subjecting

Table 1. Data Collection and Refinement Statistics

Data Collection[a]	
space group	$P2_1$
unit cell dimensions (*a*, *b*, *c*, *β*)	88.72 Å, 150.94 Å, 88.61 Å, 107.0°
completeness (%)	97.8 (95.6)
no. of reflections	131116
redundancy	3.5 (3.4)
$I/\sigma(I)$	11.02 (2.6)
R_{meas}[b] (%)	9.1 (55.8)
$R_{mrgd\text{-}F}$[c] (%)	10.8 (54.8)
Refinement	
resolution (Å)	2.08
R_{work}	0.19
R_{free}[d]	0.24
no. of atoms	
protein	13427
ligand	144
water	147
B factor (Å^2)	
protein	42.4
ligand	24.5
water	34.6
stereochemical ideality	
bond lengths (Å^2)	0.006
bond angles (deg)	0.83
φ and ψ in most favored regions (%)	97.8
φ and ψ in allowed regions (%)	2.2
φ and ψ in generously allowed regions (%)	0.0

[a]Values in parentheses are for the highest-resolution shell. [b]R_{meas} is the redundancy-independent merging *R* factor of Diederichs and Karplus.[39] [c]$R_{mrgd\text{-}F}$ is the measure of reduced data accuracy.[39] [d]Calculated posteriori R_{free} (see Materials and Methods).[16]

dx.doi.org/10.1021/bi301067w | *Biochemistry* 2012, 51, 9364−9374

the model to Cartesian simulated annealing at 5000 K as previously described.[16] Refinement statistics are listed in Table 1.

Sedimentation Velocity. Cofactor and substrate studies used 60 μM NAD^+/NADH, 50 μM UDP-sugars, and 0.9 μM hUGDH in a buffer containing 150 mM KCl and 25 mM Tris (pH 8.0). The $hUGDH_{K94E}$ (8.4 μM) and hUGDH (6.4 μM) studies used a buffer of 50 mM NaCl and 25 mM Tris (pH 8.0). The protein was loaded into 12 mm cells and analyzed in an Optima XLA analytical ultracentrifuge (Beckman Coulter) at 20 °C and 50000 rpm for 8 h. Sedimentation data for 0.9 μM hUGDH were recorded at 230 nm using a 0.003 cm step size. $hUGDH_{K94E}$ and hUGDH sedimentation was recorded at 280 nm using the same step size. SEDENTERP[17] estimated a density of 1.00603 g/mL, a viscosity of 0.010068 P, and a partial specific volume of 0.7384 mL/g for the solutions prepared at an enzyme concentration of 0.9 μM. Solutions prepared at 9.1 μM protein had a density of 1.00101 g/mL, a viscosity of 0.010142 P, and a partial specific volume of 0.7384 mL/g. Sedimentation data for all experiments were modeled to a best fit $c(s)$ distribution that fit systematic and time invariant noise as well as baseline and meniscus.[18]

Kinetics. For steady state analysis, we collected initial velocity data at the pH optimum of the enzyme [100 mM glycine (pH 8.7), 50 mM NaCl, and 5 mM EDTA]. Enzyme and substrate solutions were preincubated for 5 min at 25 °C prior to being mixed, and the reactions were monitored in a silanized 10 or 2 mm quartz cuvette. NADH production was followed at 340 nm using an Agilent 8453 UV−vis spectrometer outfitted with a Peltier temperature controller set to 25 °C. The NADH absorbance at 340 nm was converted to a molar rate using an extinction coefficient of 6220 M^{-1} cm^{-1}.[19] All initial velocities were measured during the linear phase of the reaction before 10% of the substrate had been consumed and fit to the Michaelis−Menten equation using nonlinear regression in Prism (http://www.graphpad.com/scientific-software/prism/).

***B* Factor Analysis.** All structures were re-refined without TLS[20] parameters prior to analysis. The main chain *B* factor was calculated for each residue using the program *BAVERAGE* as implemented in CCP4.[21] The *B* factors of equivalent chains in each crystal structure were averaged to reduce the effects of crystal packing. To ease comparisons, the averaged main chain *B* factors of different hUGDH crystal structures were scaled using the following relationship:[22,23]

$$\langle k\rangle B_a = B_b, \text{ where} \langle k\rangle = \frac{\sum_{i=1}^{n}\left(\frac{B_b}{B_a}\right)_i}{n} \quad (1)$$

where $\langle k\rangle$ is the mean scale factor that relates the *B* factors of the atoms in molecule A (B_a) to the equivalent atoms in molecule B (B_b). Some regions of the peptide will have real differences in flexibility because of cofactor and/or substrate binding. Such regions are not equivalent between the molecules and should not be included in the calculation of the mean scale $\langle k\rangle$. To identify regions with distinct flexibilities, we first calculated the standard deviation (σ) of $\langle k\rangle$ using all of the structurally equivalent atoms in molecules A and B. Next, we identified corresponding atoms in the two molecules that had a *B* factor ratio ($k = B_a/B_b$) outside of the range of $\langle k\rangle \pm 3\sigma$. We excluded the outliers and calculated the new $\langle k\rangle$ to scale the *B* factors of all atoms in both molecules.

RESULTS

The Cofactor Triggers the Formation of the Hexamer, but the Substrate Is Important for Stability. We used sedimentation velocity to study the effect of the cofactor and substrate on the oligomeric state of hUGDH. At a concentration of 0.9 μM, hUGDH forms a complex distribution of dimers (26%), tetramers (23%), and hexamers (51%) (Figure 2A). We have previously shown that this distribution is consistent with an association−dissociation system in rapid equilibrium.[8] The S values obtained from rapid equilibrium systems are biased by the mean of the $c(s)$ distribution,[18,24] meaning that in the following experiments, the apparent

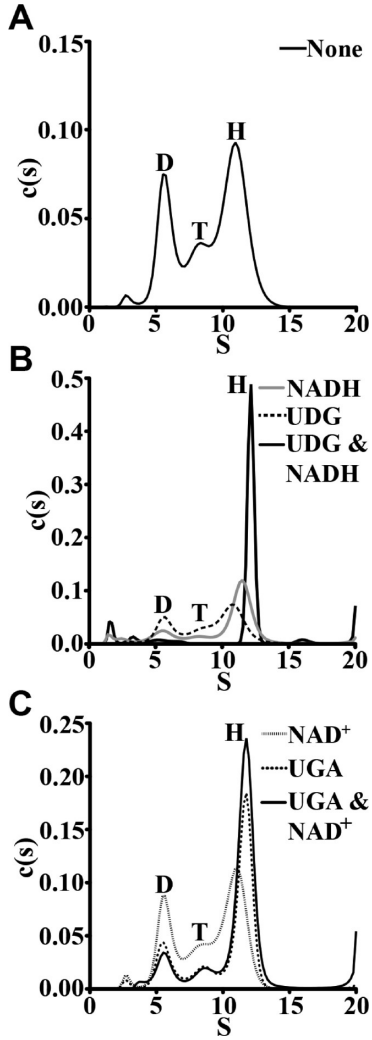

Figure 2. Effects of substrate and cofactor binding on the oligomeric state of wild-type hUGDH. (A) Sedimentation velocity results depicted as a $c(s)$ distribution.[40] hUGDH forms a distribution of dimers (D), tetramers (T), and hexamers (H) in the absence of substrates or products. The minor peak at approximately 2.8S may represent a small degree of monomer. (B) Saturating (50 μM) UDG does not shift the distribution (51% hexamer). However, saturating (60 μM) NADH shifts the distribution toward the hexameric species (70%), and the addition of 50 μM UDG with 60 μM NADH shifts the distribution almost entirely to the hexameric state (91%). (C) Subsaturating (60 μM) NAD^+ does not change the distribution (51% hexamer). UGA (50 μM) alone increases hexamer content (70%), while the addition of 60 μM NAD^+ to UGA has little if any effect on the distribution.

dx.doi.org/10.1021/bi301067w | *Biochemistry* 2012, 51, 9364−9374

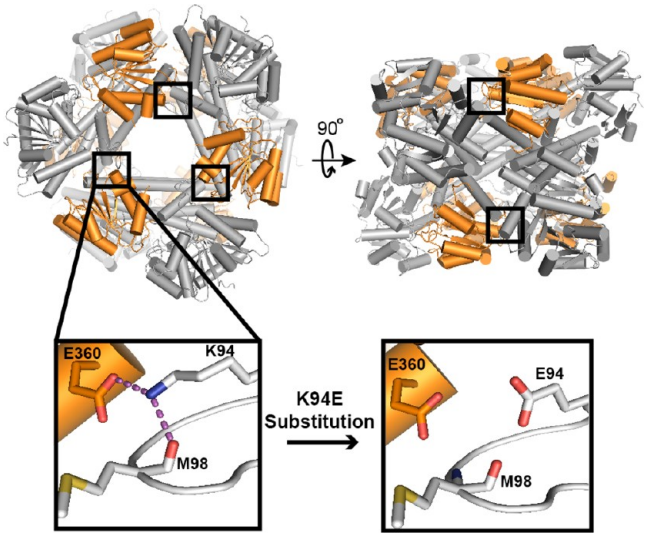

Figure 3. Design of the K94E hexamer disruption construct in hUGDH. Two views of the hUGDH hexamer related by a 90° rotation are shown in cartoon form with the SB domain colored orange and the remaining residues colored gray. Black boxes mark the substitution site in the HB interface (PDB entry 2Q3E). A magnified view (bottom left) details the interactions between K94, E360, and M98. The K94E substitution was modeled into PDB entry 2Q3E to illustrate the loss of these interactions and the introduction of an unfavorable electrostatic interaction (bottom right).

deviation in S for the hexamer (11.5S to 12.1S) does not necessarily imply a significant change in the conformation of the complex. We limited our sedimentation velocity experiments to a nucleotide concentration of ~120 μM to reduce the background absorption at 230 nm. At this concentration, NAD^+ would be subsaturating (K_d = 278 μM) so we used NADH (K_d = 4 μM)[25,26] as a cofactor analogue. At the saturating concentration of 60 μM NADH, the distribution shifted to favor an 11.5S hexamer (70% of the distribution) (Figure 2B). As expected, the equivalent (but subsaturating) concentration of NAD^+ has no significant effect on the distribution (Figure 2C). Saturation of hUGDH with both 50 μM UDG (K_d = 33)[27] and 60 μM NADH shifts the distribution almost entirely (91%) to a 12.1S hexamer (Figure 2B). In contrast, we have previously shown that UDG alone does not change the enzyme distribution[8] (Figure 2B), implying that UDG has an indirect effect on hexamer stability (see Discussion). Surprisingly, the product UGA (K_d = 13.6)[28] at 50 μM shifts (70%) the distribution into an 11.7S hexameric species (Figure 2C). The addition of subsaturating 60 μM NAD^+ has only a small effect on the UGA-stabilized hexamer (Figure 2C). Because NAD^+ is not saturating, we cannot directly compare the sedimentation velocity results of the hUGDH:UGA:NAD^+ and hUGDH:UDG:NADH experiments.

The Hexamer Is the Catalytically Relevant State. We addressed the role of the hexamer in the hUGDH mechanism by introducing the K94E substitution. K94 is located in the HB interface and forms an intersubunit salt bridge with E360 from the adjacent dimer (Figure 3). The K94E charge-switch substitution breaks the salt bridge and introduces an unfavorable electrostatic interaction with E360 that should prevent hexamer formation. The $hUGDH_{K94E}$ construct is expressed as a soluble protein at levels similar to that of wild-type hUGDH (~25 mg/L). Sedimentation velocity confirms that $hUGDH_{K94E}$ is a stable 5.8S dimer at an enzyme

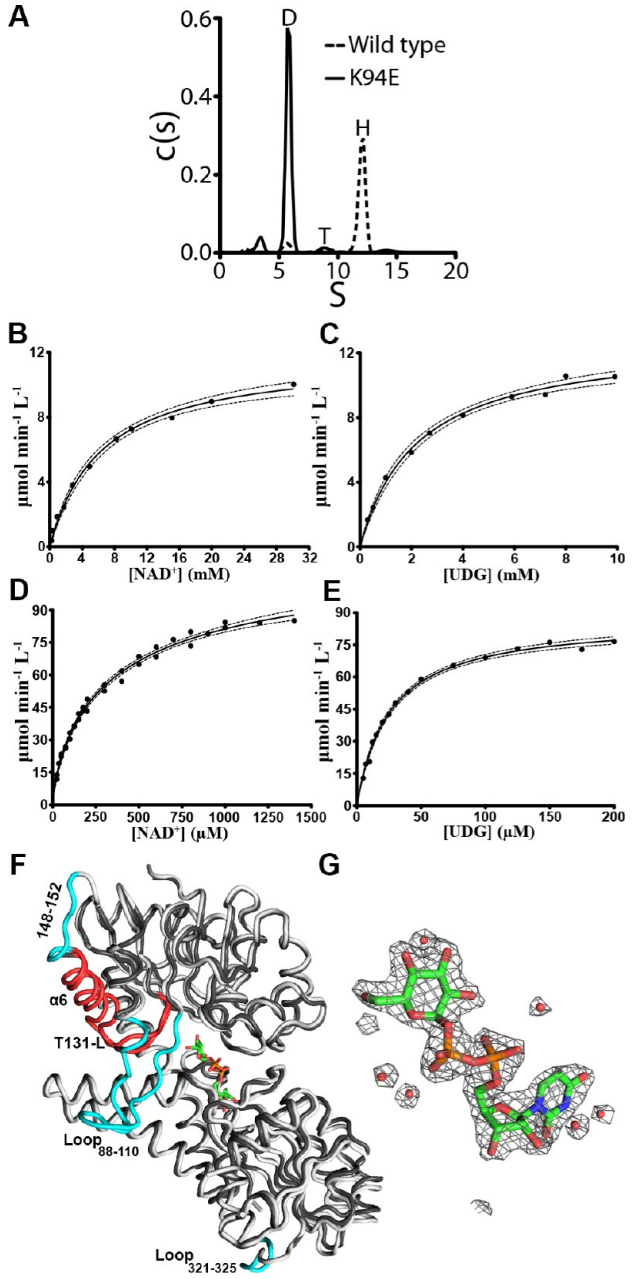

Figure 4. $hUGDH_{K94E}$ is a stable dimer with low activity. (A) Sedimentation velocity displayed as a $c(s)$ distribution shows the oligomeric states of wild-type hUGDH (6.4 μM, dashed line) and $hUGDH_{K94E}$ (8.4 μM, solid line). $hUGDH_{K94E}$ remains a dimer under conditions that favor the hexamer in wild-type hUGDH. (B and C) Substrate saturation curves of $hUGDH_{K94E}$ fit to the Michaelis–Menten equation. Dotted lines estimate the 95% confidence level of the fit line falling within the true value. (D and E) Substrate saturation curves of wild-type hUGDH fit as described above. (F) Structure of $hUGDH_{K94E}$ (dark gray) superimposed onto wild-type hUGDH (light gray, PDB entry 2Q3E). Areas of disorder in $hUGDH_{K94E}$ are colored teal on the wild-type structure. α6 helix and the Thr131-loop are colored red. (G) A $hUGDH_{K94E}$ difference ($F_o - F_c$) electron density map calculated at the 3σ level after UDG had been omitted and the model had been subjected to simulated annealing.

concentration of 8.4 μM (Figure 4A). At a concentration of 6.4 μM, wild-type hUGDH is stable as a 12.2S hexamer (Figure 4A). The steady state kinetics of $hUGDH_{K94E}$ shows that the K_m for NAD^+ and UDG has increased by ~16- and ~88-fold,

dx.doi.org/10.1021/bi301067w | Biochemistry 2012, 51, 9364–9374

Table 2. Kinetic Comparison of K94E to Wild-Type hUGDH

	K_m (μM)		k_{cat} (min^{-1})	
	NAD^+	UDG	NAD^+	UDG
wild type	384 ± 75	25.3 ± 1.2	262.9 ± 17.3	188.7 ± 2.8
$hUGDH_{K94E}$	6300 ± 561	2210 ± 188	1.30 ± 0.04	1.41 ± 0.04

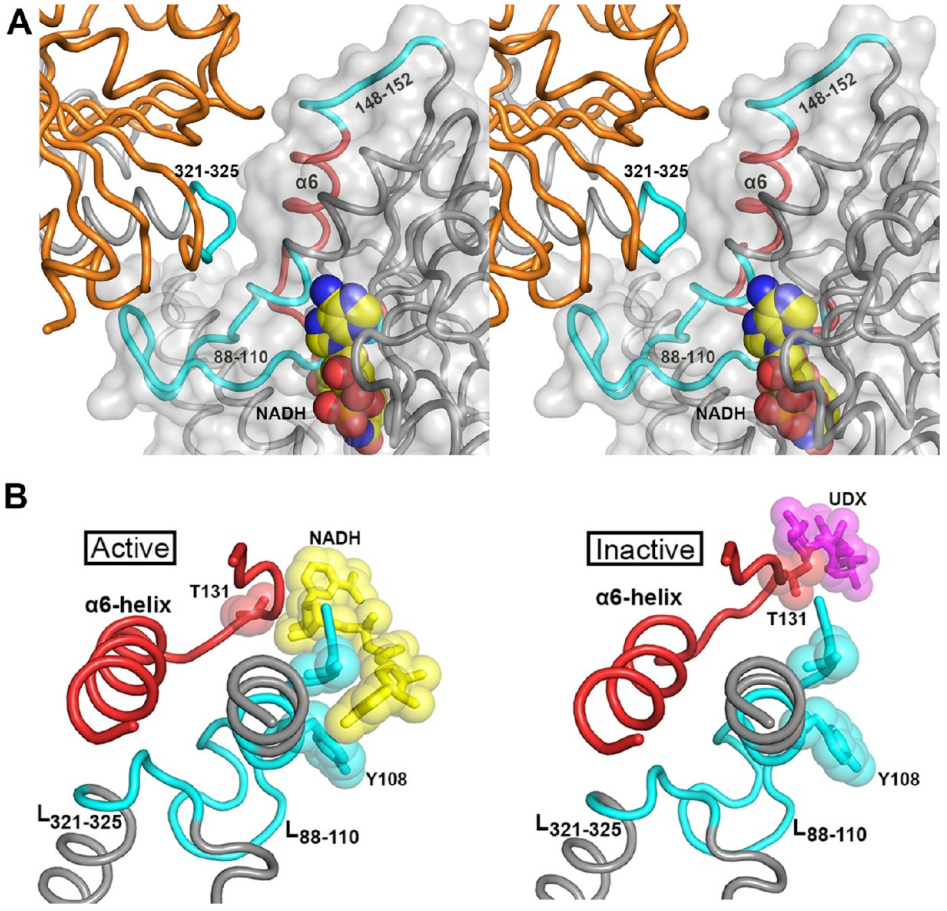

Figure 5. $Loop_{88-110}$ and the Thr131-loop/α6 helix form the HB interface. (A) Stereodiagram depicting the complementary packing interactions that form the HB interface between the NB (gray) and SB (orange) domains of adjacent dimers (PDB entry 2Q3E). The molecular surface (translucent gray) of the NB domain is depicted with bound NADH (yellow carbons). The Thr131-loop/α6 helix is colored in red, and loops disordered in $hUGDH_{K94E}$ are colored teal. (B) $Loop_{88-110}$ (teal) and the Thr131-loop/α6 helix (red) allosteric switches interact with each other to form the HB interface. The active conformation corresponds to the 32 symmetry hexamer (PDB entry 2Q3E) and shows that NADH (yellow) packs against $loop_{88-110}$ and the Thr131-loop to indirectly buttress the HB interface. The inactive conformation depicts UDX (purple) interacting with the Thr131-loop to form the HB interface corresponding to the horseshoe-shaped hexamer (PDB entry 3PTZ).

respectively (Table 2 and Figure 4B–E). In addition, the k_{cat} for $hUGDH_{K94E}$ is ~160 times slower than that of the wild-type enzyme. Because the K94E substitution is ~17 Å from the active site, the changes in substrate affinity and enzyme activity are most likely due to the loss of the hexameric assembly (see Discussion).

$Loop_{88-110}$ and the Thr131-loop/α6 Helix Link Cofactor Binding to the Hexamer-Building Interface. We determined the crystal structure of $hUGDH_{K94E}$ in complex with UDG at 2.08 Å resolution, revealing two dimers in the asymmetric unit (Figure 4F,G). The NB and SB domains of the $hUGDH_{K94E}$:UDG complex are in the "closed" conformation (Figure 1B). The four copies of the $hUGDH_{K94E}$:UDG complex superimpose with root-mean-square deviations (rmsd) of <0.2 Å for 422 corresponding Cα atoms. With the exception of four disordered loops, all residues are modeled in the structure. The first two disordered loops (residues 148–152 and 466–494) are frequently missing in hUGDH crystal structures (Figure 4F). The two remaining disordered loops, $loop_{88-110}$ and $loop_{321-325}$, form the HB interface in the hexameric complex. The hUGDH structure has already been described in detail,[8−11] so we will focus our analysis on conformational changes associated with hexamer formation and cofactor binding.

Dimeric $hUGDH_{K94E}$ superimposes onto the hUGDH:UDG:NADH hexamer (PDB entry 2Q3E) with an rmsd of 0.7 Å for 427 corresponding Cα atoms. The hUGDH:UDG:NADH structure shows that $loop_{88-110}$ represents 398 $Å^2$, or 61% of the total buried surface area in the HB interface (Figure 5A). $Loop_{88-110}$ and the Thr131-loop/α6 helix combine to form a complementary packing surface with $loop_{321-325}$ in the HB interface (Figure 5B). We have previously identified the Thr131-loop/α6 helix element as the allosteric switch that responds to the feedback inhibitor UDX to produce the

dx.doi.org/10.1021/bi301067w | Biochemistry 2012, 51, 9364–9374

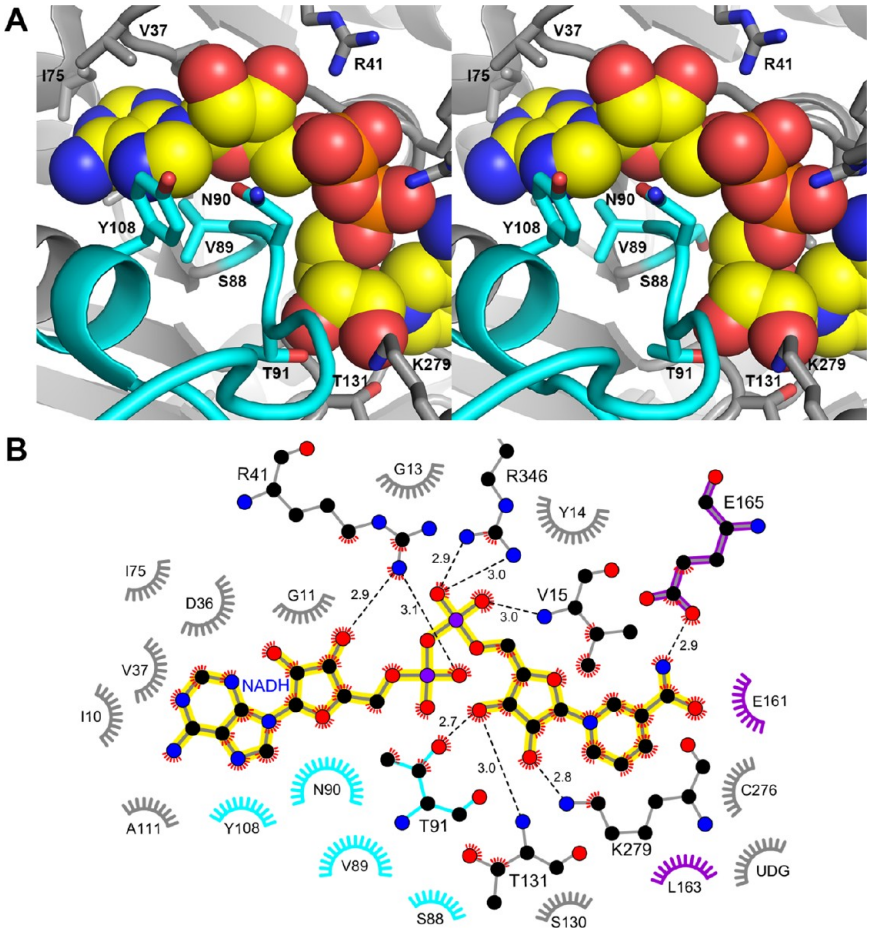

Figure 6. $Loop_{88-110}$ interacts with the bound cofactor NAD(H). (A) Stereoview of the cofactor binding site revealing the interactions between the bound NADH (yellow carbons) and $loop_{88-110}$ (teal sticks and cartoon main chain) in the hUGDH:UDG:NADH complex (PDB entry 2Q3E). (B) Ligplot[41] representation showing the packing interactions (feathered lines) and hydrogen bonds (dotted lines) of the cofactor with the protein. $Loop_{88-110}$ residues are colored teal, and S-loop residues are colored magenta.

horseshoe-shaped hexamer (see Discussion).[8,9] Briefly, UDX binding induces the Thr131-loop to move ~4 Å into the active site cleft, rotating α6 helix to produce the inactive hexamer (Figure 5B).

$Loop_{88-110}$ and the Thr131-loop/α6 helix also directly interact with the cofactor in the 32 symmetry hexamer (Figures 5 and 6). Residues 88−91 form a surface that supports NAD^+ binding, and Tyr108 packs against the edge of the adeninosyl ring (Figure 6A,B). In addition to packing interactions, the Thr91 Oγ atom forms a hydrogen bond with the O3′ atom of the nicotinamide ribosyl. Thr131 also packs against the nicotinamide ribosyl and donates a hydrogen from the main chain amide to the to the O3′ atom of the nicotinamide ribosyl (Figure 6B).

The Flexibility of the HB Interface Changes with Domain Rotation. Our earlier work showed that the packing of the Thr131-loop/α6 helix in the HB interface is sensitive to the conformation of the NB domain.[9] Here we compare the conformation of the NB and SB domains with the flexibility of the HB interface using the hUGDH:UGA:NAD^+ crystal structure (PDB entry 2GQ4). The hUGDH:UGA:NAD^+ complex contains four asymmetric dimers; each dimer has one subunit in the open domain conformation (chains A, C, E, and G) and the other in the closed state (chains B, D, F, and H).[9] Application of crystal symmetry transforms each dimer into an asymmetric hexamer (Figure 7A, inset). Using main chain crystallographic *B* factors, we identify flexible regions of the structure. Molecules with domains in the same conformation display a similar pattern of flexibility (Figure 7A). In contrast, comparing the *B* factors of the molecules with domains in the open conformation to those with closed domains reveals significant changes in the HB interface. The open conformation is correlated with an increase in the *B* factors of $loop_{88-110}$, the Thr131-loop/α6 helix, and a substrate binding loop that we call the "S-loop" (residues 157−172) (Figures 7A and 8). Because rotation of the domains alters the packing interactions in the HB interface, the change in flexibility for $loop_{88-110}$ and the Thr131-loop/α6 helix was expected. However, the S-loop interacts with the substrate and cofactor in the active site and is not involved in the HB interface (Figure 8). The S-loop forms a complementary packing surface and contributes hydrogen bonds to UDG and NAD^+. The increased flexibility of the S-loop in the open conformation is also reflected in the disorder of the nicotinamide and ribosyl of NAD^+ (not shown). The ordering of the active site as the domains rotate to a closed conformation is consistent with an induced-fit mechanism for cofactor binding.

Cofactor and Substrate Binding Creates a More Rigid Hexamer-Building Interface. In each of the following analyses, we compare structures with domains only in the closed conformation. We first examined the effect of mixed

dx.doi.org/10.1021/bi301067w | *Biochemistry* 2012, 51, 9364−9374

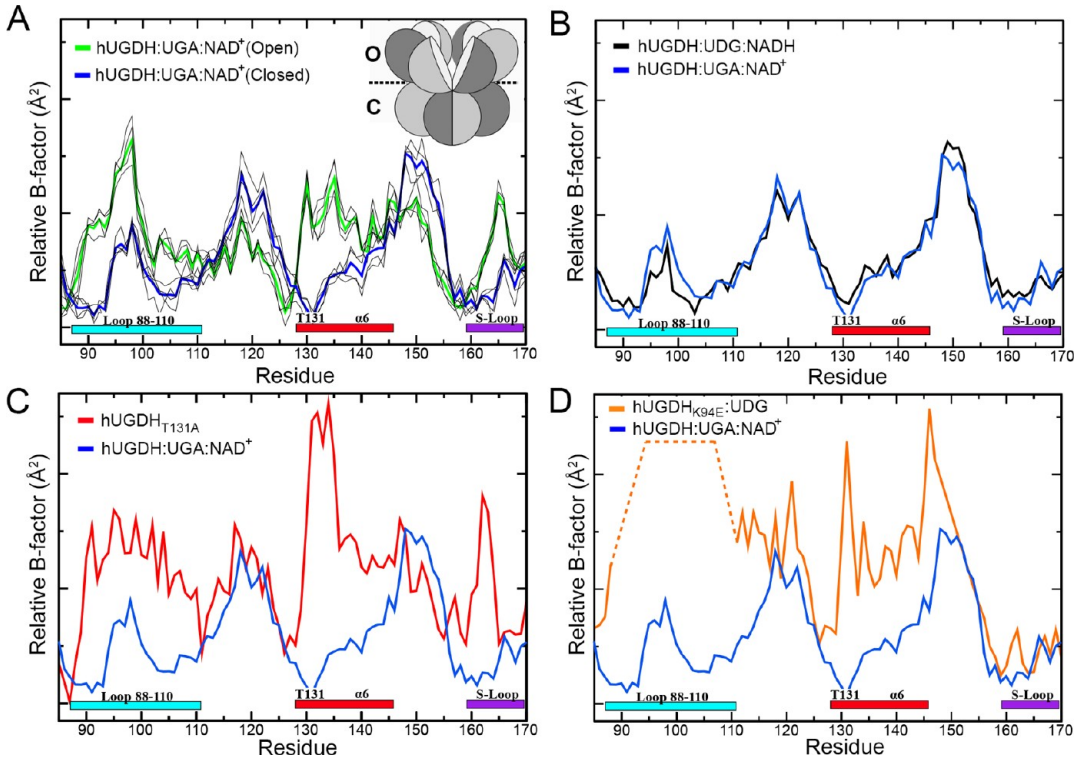

Figure 7. Domain closure and substrate binding decrease the flexibility of hUGDH. (A) The NB and SB domains of the hUGDH:UGA:NAD$^+$ complex (PDB entry 2QG4) display an open−closed asymmetry between the top and bottom trimers of the hexamer (inset cartoon). A plot of main chain *B* factors for residues 85−170 indicates the relative flexibility of loop$_{88-110}$ (teal bar), the Thr131-loop/α6 helix (red bar), and the S-loop (magenta bar). Thick colored lines indicate the averaged main chain *B* factors for the open (green) and closed (blue) conformations. Thin gray lines show the *B* factors of individual chains to illustrate the small differences caused by crystal packing. (B) The mixed substrate−product ternary complexes, hUGDH:UDG:NADH and hUGDH:UGA:NAD$^+$, have similar degrees of order in the HB interface and the S-loop. (C) The structure of hUGDH$_{T131A}$ (PDB entry 3ITK) shows that the HB interface and S-loop become disordered in the absence of the cofactor and substrate. (D) The HB interface of dimeric hUGDH$_{K94E}$ (orange) is disordered. Dashed lines indicate unmodeled loop$_{88-110}$. To ease comparison, all *B* factors in this figure were scaled to chain A of PDB entry 2Q3E (see Materials and Methods).

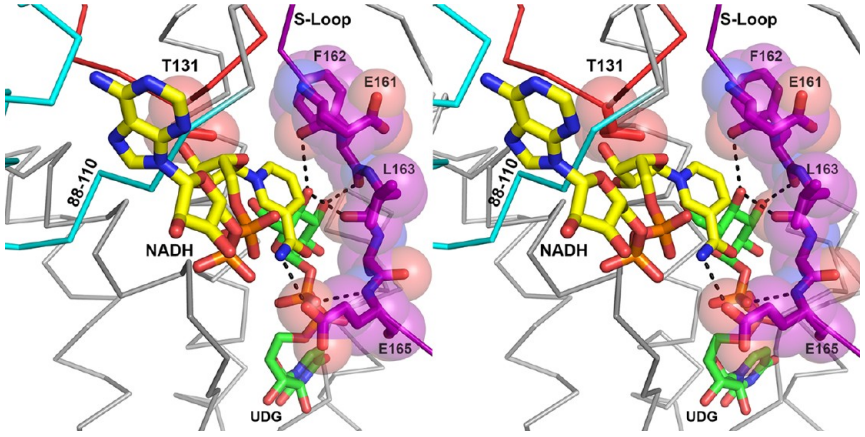

Figure 8. Stereodiagram showing that the S-loop interacts with the substrate and cofactor. The S-loop (shown as magenta spheres and sticks) interacts with UDG (green carbons) and NADH (yellow carbons). Loop$_{88-110}$ (teal trace) and the Thr131-loop/α6 helix (red trace) are also depicted. Some residues have been removed to provide a clear view of the buried binding pocket.

substrate−product ternary complexes on the flexibility of the active site and the HB interface. The crystal structures of the hUGDH:UGA:NAD$^+$ and hUGDH:UDG:NADH complexes (12 molecules in the asymmetric unit, PDB entry 2Q3E) revealed no significant differences in *B* factor analysis (Figure 7B). This means the substrate and product have similar effects on main chain flexibility. This analysis also shows that differences in the crystallization conditions and space group have little to no effect on the flexibility of the HB interface.

Next, we considered how the absence of the cofactor and substrate affects the flexibility of the active site and the HB interface. The crystal structure of the hUGDH$_{T131A}$ hexamer (PDB entry 3ITK) does not contain the cofactor or substrate and reveals a sharp increase in the flexibility of the S-loop (Figure 7C). This is consistent with the loss of favorable

dx.doi.org/10.1021/bi301067w | *Biochemistry* 2012, 51, 9364−9374

packing interactions in the active site. $Loop_{88-110}$ and the Thr131-loop/α6 helix are also more flexible in the absence of the cofactor and substrate. This demonstrates a direct link between cofactor−substrate binding in the active site and packing in the HB interface.

Finally, we examined the crystal structure of dimeric $hUGDH_{K49E}$ in complex with UDG to gain insight into the conformational changes that precede hexamer formation (Figure 7D). In the dimer, $loop_{88-110}$ is disordered and the Thr131-loop/α6 helix is more flexible in the absence of the cofactor. This implies that hexamer formation is accompanied by a disorder-to-order transition. This analysis also shows that UDG binding alone can order the S-loop, suggesting that the substrate can facilitate the binding of the cofactor. The disorder of $loop_{88-110}$ and the Thr131-loop/α6 helix in the $hUGDH_{K49E}$:UDG complex means there is no direct link between the substrate and the HB interface.

DISCUSSION

Sequential Binding of UDG and the Cofactor Triggers Formation of the Active 32 Symmetry Hexamer. We have previously shown that hUGDH exists as a concentration-dependent distribution of dimers, tetramers, and hexamers in rapid equilibrium.[8] We have now extended those studies to show that the 32 symmetry hexamer is the catalytically important oligomeric state. Our $hUGDH_{K94E}$ construct forms a stable dimer that is ∼160-fold less active than the wild-type enzyme (Figure 4B−E). Because the K94E substitution is ∼17 Å from the active site, the loss of activity implies that the hexamer is the catalytically relevant oligomeric state. It is possible that the loss of activity in the $hUGDH_{K94E}$ dimer is due to an unexpected long-range effect of the K94E substitution on the catalytic mechanism, but we do not believe that this is the case. First, we observe that hexamer formation stabilizes the active site Figure 7d). Second, we also show that the flexibility of the active site in the hUGDH:UGA:NAD^+ hexamer is directly correlated with the conformation of the hexamer-building interface (Figure 7a). This is good evidence of a direct link between the active site and the packing interactions in the hexamer-building interface.

We have also shown that binding of the cofactor triggers hexamer formation (Figure 2B). We chose NADH as a cofactor analogue for two reasons. (i) NADH has a binding affinity ∼55 times greater than that of NAD^+, allowing us to saturate hUGDH well below the ∼120 μM nucleotide limit imposed by the sedimentation velocity experiment. (ii) The closed conformations of the hUGDH:UGA:NAD^+ and hUGDH:UDG:NADH crystal structures are very similar in structure and disorder, and the cofactors NADH and NAD^+ engage in very similar interactions.[9,10] Still, the fact that hUGDH has a higher affinity for NADH suggests that cofactor binding may be accompanied by small but significant differences in conformation or dynamics that are not apparent in the available crystal structures. Because NADH drives hexamer formation, we would assume that the reported K_d to corresponds to the hexameric state and the dimer has a weaker affinity for NADH. This is supported by our observation that the K_m of the $hUGDH_{K94E}$ dimer for NAD^+ is ∼16-fold higher than that of the wild-type enzyme (Table 2). In addition, the K_m for UDG is ∼88-fold higher in $hUGDH_{K94E}$, suggesting that the hexameric assembly also facilitates binding of the sugar substrate.

Our analysis of the hUGDH crystal structures identifies the mechanism by which cofactor binding can trigger hexamer formation. Because $loop_{88-110}$ and the Thr131-loop/α6 helix interact directly with the cofactor (Figures 5 and 8) and also pack together to form the HB interface, they are obvious candidates for the cofactor-responsive allosteric switch (Figures 5 and 6). In support of this hypothesis, we show that cofactor and substrate binding reduces the flexibility of $loop_{88-110}$ and the Thr131-loop/α6 helix in the HB interface (Figure 7C). A more rigid HB interface upon binding of the substrate and cofactor may contribute to the increased stability of the hexamer that we observe in solution studies (Figure 2B). In addition, $loop_{88-110}$ is completely disordered and the Thr131-loop/α6 helix is very flexible in the dimeric state of hUGDH (Figure 7D). These observations support a mechanism whereby cofactor binding promotes the local folding of $loop_{88-110}$ and buttresses the Thr131-loop/α6 helix to form a rigid HB interface that triggers hexamer formation (Figures 5 and 6).

While cofactor binding is the event that triggers hexamer formation, UDG is important for the stability of the complex (Figure 2B). Because UDG binding alone does not promote hexamer formation,[8] the substrate has an indirect effect on hexamer stability (Figure 2B). We have identified the structural basis for the indirect mechanism by which UDG stabilizes the hUGDH:UDG:NADH hexamer. In the active site, the S-loop interacts with both UDG and NAD(H) (Figure 8). A comparison of the $hUGDH_{K94E}$:UDG complex to the hUGDH:UDG:NADH hexamer shows that UDG binding alone can stabilize the S-loop, which would improve the affinity of hUGDH for the cofactor (Figure 7D). In fact, recent binding studies in our lab show that UDG increases the affinity of hUGDH for NADH by a factor of ∼8 (manuscript in preparation). Thus, UDG indirectly contributes to hexamer stability by enhancing the binding of the cofactor. Our observation that UDG promotes cofactor binding supports the sequential, ordered mechanism that has been proposed for UGDH.[29,30]

Finally, we report that the flexibility of the HB interface is strongly correlated with the conformation of the NB and SB domains of hUGDH. During the catalytic cycle, the domains rotate to release products and bind the substrate (Figure 1B).[9,10] In the open conformation, the active site and the HB interface are very flexible (Figure 7A). As the domains rotate to the closed conformation, the HB interface and active site become more rigid. This is good evidence of an induced-fit conformational change that can stabilize the hexameric assembly during catalytic turnover.

A Plausible Model for the hUGDH Catalytic Cycle in the Crowded Environment of a Cell. The preceding analysis supports the following model. (1) The binding of UDG to the hUGDH dimer results in the ordering of the S-loop and the subsequent binding of the cofactor. (2) Cofactor binding followed by domain closure stabilizes $loop_{88-110}$ and the Thr131-loop/α6 helix to trigger the formation of the catalytically active hexamer. This model is consistent with the sequential, ordered mechanism of UGDH,[29,30] but we do not believe it represents the hUGDH catalytic cycle in a living cell. The highly crowded cytosolic environment (∼200−320 mg/mL of protein)[31,32] will stabilize the hexamer and prevent it from undergoing significant dissociation.[33−35] Thus, the association−dissociation behavior we observe is a consequence of assaying hUGDH under dilute conditions. It is unlikely that the dimer plays a significant role in the catalytic cycle. Instead, we believe that the cofactor-induced rigidity of the HB interface is part of an induced fit response (Figure 9A, step 1→ 2a).

dx.doi.org/10.1021/bi301067w | Biochemistry 2012, 51, 9364−9374

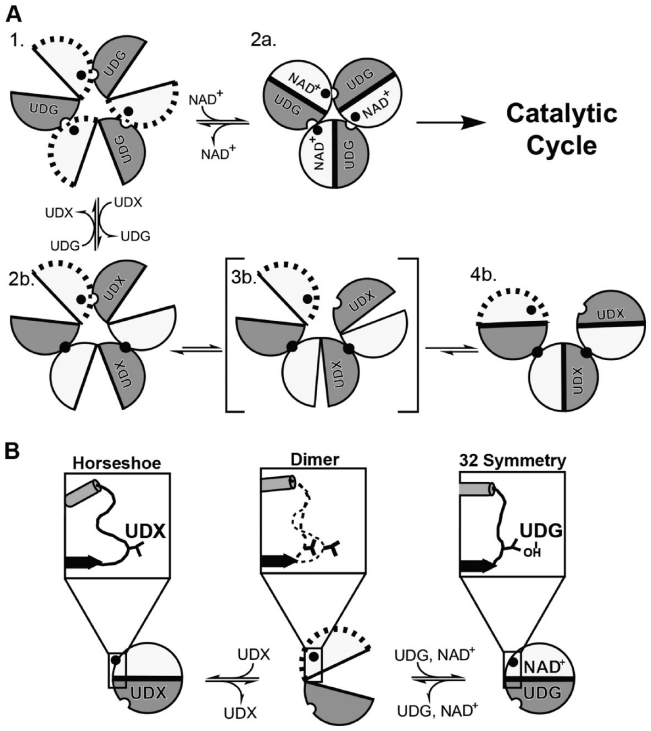

Figure 9. Cartoon model for the catalytic cycle of hUGDH. (A) For the sake of clarity, only the top trimer of the hUGDH hexamer is shown, with the NB and SB domains depicted as white and gray semicircles, respectively. Disorder of $loop_{88-110}$ is shown as a dotted outline of the NB domain. The Thr131-loop/α6 helix is depicted as a small black circle in the NB domain, and the semicircle cutout in the SB domain represents $loop_{321-325}$ that interacts with the α6 helix (see Figure 5). In step 1, in the absence of the cofactor, the HB interface is disordered but hUGDH is maintained in the hexameric state by the crowding conditions of the cell. In step 2a, binding of the cofactor promotes ordering of $loop_{88-110}$ and the induced fit closing of the NB domains to form the catalytically active complex. In step 2b, the UDX inhibition mechanism has been previously described.[9] Here we modify it to incorporate disordered $loop_{88-110}$. Briefly, UDX competes with UDG binding to shift the Thr131-loop/α6 helix (black circle) and strengthen the packing interactions with $loop_{321-325}$ (semicircle cutout). This model assumes that substoichiometric binding of UDX will strengthen two of the three interfaces. In step 3b, as the remaining weak interface dissociates, the UDX-containing subunits will rotate closed to maximize interactions with the feedback inhibitor, forming in step 4b the horseshoe-shaped complex. (B) Detailed interactions between the Thr131-loop/α6 helix and UDX or UDG/NAD^+ binding. A single chain of hUGDH is represented as two semicircles colored as described above. In the absence of the ligand, the NB and SB domains are in an open conformation and the Thr131-loop (inset) and $loop_{88-110}$ are disordered. The binding of UDX stabilizes an extended Thr131-loop conformation that has a rotated α6 helix (small dot) and a more stable HB interface to form the inactive complex. The substrate UDG has a 5′-hydroxymethyl (OH, inset box) not found in UDX. This hydroxymethyl locks the Thr131-loop in a conformation that favors the active state of the enzyme. The binding of the cofactor also stabilizes $loop_{88-110}$ and buttresses the Thr131-loop/α6 helix to induce formation of the 32 symmetry hexamer.

When the NB and SB domains are in the open conformation, the active site and the HB interface are flexible (Figure 7A). The flexibility of the HB interface is important to allow the NB and SB domains to rotate without disrupting the hexamer.[9] When the substrate binds, $loop_{88-110}$ and the Thr131-loop/α6 helix become rigid as the domains rotate to form the closed conformation (Figure 9A, step 1 → 2a).

The Thr131-loop/α6 helix is also the allosteric switch that responds to the feedback inhibitor UDX.[8,9] Briefly, UDX competes with the substrate UDG for the active site (Figure 9B). When UDX binds to the SB domain, the absence of a C5′ hydroxymethyl (the only difference between inhibitor and substrate) induces the Thr131-loop/α6 helix in the NB domain to undergo a change in conformation (Figure 9B).[8] This allosteric transition produces a stable HB interface with a conformation that favors the horseshoe-shaped hexamer (Figures 6 and 9A, step 1 → 2b). We have previously shown[9] that the UDX-like HB interface can occur in the 32 symmetry hexamer, but only when the domains are rotated open (Figure 9A, step 1 → 2b). A 32 hexamer not fully saturated with UDX will preferentially dissociate along one of the weaker HB interfaces as the domains rotate to form the closed conformation, creating the horseshoe-shaped hexamer (Figure 9A, step 2b → 4b).

The crystal structure of the asymmetric hUGDH:UGA:NAD^+ complex was important because it allowed us to analyze the contribution of the domain conformation to the stability of the HB interface (Figure 7A). It has not escaped our notice that the hUGDH:UGA:NAD^+ complex is also consistent with earlier reports of half-of-the-sites activity for hUGDH.[36−38] Half-of-the-sites activity means that only 50% of the active sites turn over at any time and the crystal structure would be expected to show asymmetry (Figure 7A, inset). While the hUGDH:UGA:NAD^+ structure is consistent with a half-of-the-sites mechanism, none of the other hUGDH structures show this type of asymmetry. This apparent contradiction may be linked to the distinct effects of UDG and UGA on hexamer stability; UDG has no effect on hexamer stability, but UGA can induce hexamer formation (Figure 2A,C). Because UGA does not interact with $loop_{88-110}$ in the active site, the hexamer stabilization is distinct from the cofactor-induced mechanism. A precedent for the UGA-induced hexamer may be found in the mechanism by which the structurally similar feedback inhibitor UDX promotes hexamer formation without directly interacting with $loop_{88-110}$ (Figure 9B).[8,9] It may be that UGA alters the Thr131-loop/α6 helix to stabilize the asymmetric hexamer. Unfortunately, the hUGDH:UGA:NAD^+ crystal structure is only part of the picture needed to understand how the UGA-induced hexamer is stabilized and the source of the asymmetry. There is need for a crystal structure of the hUGDH−UGA complex to determine the mechanism behind the UGA-induced asymmetric hexamer.

■ ASSOCIATED CONTENT

Accession Codes

The atomic coordinates and structure factors have been deposited in the Protein Data Bank as entry 4EDF.

■ AUTHOR INFORMATION

Corresponding Author

*Phone: (706) 583-0304. Fax: (706) 542-1738. E-mail: zac@bmb.uga.edu.

Funding

Funding from American Cancer Society Grant RSG0918401DMC and the University of Georgia Research Alliance to Z.A.W. is gratefully acknowledged.

Notes

The authors declare no competing financial interest.

■ ABBREVIATIONS

hUGDH, human UDP-α-D-glucose-6-dehydrogenase; HB, hexamer-building; NB, NAD^+ binding; SB, UDP sugar binding; UDE, UDP-α-D-6-thio-gluco-hexodialdo-1,5-pyranose; UDH, UDP-α-D-6-thio-glucose; UDG, UDP-α-D-glucose; UGA, UDP-α-D-glucuronic acid; UDX, UDP-α-D-xylose.

■ REFERENCES

(1) Axelrod, J., Kalckar, H. M., Maxwell, E. S., and Strominger, J. L. (1957) Enzymatic formation of uridine diphosphoglucuronic acid. *J. Biol. Chem. 224*, 79−90.

(2) Tukey, R. H., and Strassburg, C. P. (2000) Human UDP-glucuronosyltransferases: Metabolism, expression, and disease. *Annu. Rev. Pharmacol. Toxicol. 40*, 581−616.

(3) Cummings, J., Zelcer, N., Allen, J., Yao, D., Boyd, G., Maliepaard, M., Friedberg, T., Smyth, J., and Jodrell, D. (2004) Glucuronidation as a mechanism of intrinsic drug resistance in colon cancer cells: Contribution of drug transport proteins. *Biochem. Pharmacol. 67*, 31−39.

(4) Cummings, J., Ethell, B., Jardine, L., Boyd, G., Macpherson, J., Burchell, B., Smyth, J., and Jodrell, D. (2003) Glucuronidation as a mechanism of intrinsic drug resistance in human colon cancer: Reversal of resistance by food additives. *Cancer Res. 63*, 8443.

(5) Oguri, T., Takahashi, T., Miyazaki, M., Isobe, T., Kohno, N., Mackenzie, P. I., and Fujiwara, Y. (2004) UGT1A10 is responsible for SN-38 glucuronidation and its expression in human lung cancers. *Anticancer Res. 24*, 2893−2896.

(6) Takahashi, T., Fujiwara, Y., Yamakido, M., Katoh, O., Watanabe, H., and Mackenzie, P. I. (1997) The role of glucuronidation in 7-ethyl-10-hydroxycamptothecin resistance in vitro. *Jpn. J. Cancer Res. 88*, 1211−1217.

(7) de Almagro, M. C., Selga, E., Thibaut, R., Porte, C., Noe, V., and Ciudad, C. J. (2011) UDP-glucuronosyltransferase 1A6 overexpression in breast cancer cells resistant to methotrexate. *Biochem. Pharmacol. 81*, 60−70.

(8) Kadirvelraj, R., Sennett, N. C., Polizzi, S. J., Weitzel, S., and Wood, Z. A. (2011) Role of packing defects in the evolution of allostery and induced fit in human UDP-glucose dehydrogenase. *Biochemistry 50*, 5780−5789.

(9) Sennett, N. C., Kadirvelraj, R., and Wood, Z. A. (2011) Conformational flexibility in the allosteric regulation of human UDP-α-D-glucose 6-dehydrogenase. *Biochemistry 50*, 9651−9663.

(10) Egger, S., Chaikuad, A., Kavanagh, K. L., Oppermann, U., and Nidetzky, B. (2011) Structure and mechanism of human UDP-glucose 6-dehydrogenase. *J. Biol. Chem. 286*, 23877−23887.

(11) Egger, S., Chaikuad, A., Klimacek, M., Kavanagh, K. L., Oppermann, U., and Nidetzky, B. (2011) Structural and kinetic evidence that the catalytic reaction of human UDP-glucose 6-dehydrogenase involves covalent thiohemiacetal and thioester enzyme intermediates. *J. Biol. Chem. 287*, 2119−2129.

(12) Kabsch, W. (2010) XDS. *Acta Crystallogr. D66*, 125−132.

(13) Adams, P. D., Afonine, P. V., Bunkóczi, G., Chen, V. B., Davis, I. W., Echols, N., Headd, J. J., Hung, L.-W., Kapral, G. J., Grosse-Kunstleve, R. W., McCoy, A. J., Moriarty, N. W., Oeffner, R., Read, R. J., Richardson, D. C., Richardson, J. S., Terwilliger, T. C., and Zwart, P. H. (2010) PHENIX: A comprehensive Python-based system for macromolecular structure solution. *Acta Crystallogr. D66*, 213−221.

(14) Vagin, A., and Teplyakov, A. (2010) Molecular replacement with MOLREP. *Acta Crystallogr. D66*, 22−25.

(15) Emsley, P., and Cowtan, K. (2004) Coot: Model-building tools for molecular graphics. *Acta Crystallogr. D60*, 2126−2132.

(16) Brunger, A. T., and Rice, L. M. (1997) Crystallographic refinement by simulated annealing: Methods and applications. *Methods Enzymol. 277*, 243−269.

(17) Laue, T., Shah, B., Ridgeway, T., and Pelletier, S. (1992) Computer-aided interpretation of analytical sedimentation data for proteins. In *Analytical ultracentrifugation in biochemistry and polymer science* (Harding, S. E., Rowe, A. J., and Horton, J. C., Eds.) The Royal Society of Chemistry, Cambridge, U.K.

(18) Schuck, P. (2003) On the analysis of protein self-association by sedimentation velocity analytical ultracentrifugation. *Anal. Biochem. 320*, 104−124.

(19) Haid, E., Lehmann, P., and Ziegenhorn, J. (1975) Molar absorptivities of β-NADH and β-NAD at 260 nm. *Clin. Chem. 21*, 884−887.

(20) Schomaker, V., and Trueblood, K. N. (1968) On the rigid-body motion of molecules in crystals. *Acta Crystallogr. B24*, 63−76.

(21) Winn, M. D., Ballard, C. C., Cowtan, K. D., Dodson, E. J., Emsley, P., Evans, P. R., Keegan, R. M., Krissinel, E. B., Leslie, A. G. W., McCoy, A., McNicholas, S. J., Murshudov, G. N., Pannu, N. S., Potterton, E. A., Powell, H. R., Read, R. J., Vagin, A., and Wilson, K. S. (2011) Overview of the CCP4 suite and current developments. *Acta Crystallogr. D67*, 235−242.

(22) Wood, Z. A., Poole, L. B., Hantgan, R. R., and Karplus, P. A. (2002) Dimers to Doughnuts: Redox-Sensitive Oligomerization of 2-Cysteine Peroxiredoxins. *Biochemistry 41*, 5493−5504.

(23) Wood, Z., Schroder, E., and Harris, J. R. (2003) Structure, mechanism and regulation of peroxiredoxins. *Trends Biochem. Sci. 28*, 32−40.

(24) Zhao, H., Balbo, A., Brown, P. H., and Schuck, P. (2011) The boundary structure in the analysis of reversibly interacting systems by sedimentation velocity. *Methods 54*, 16−30.

(25) Franzen, J., Marchetti, P., Lockhart, A., and Feingold, D. (1983) Special effects of UDP-sugar binding to bovine liver uridine diphosphoglucose dehydrogenase. *Biochim. Biophys. Acta 746*, 146−153.

(26) Gainey, P. A., and Phelps, C. F. (1974) The binding of oxidized and reduced nicotinamide-adenine dinucleotides to bovine liver uridine diphosphate glucose dehydrogenase. *Biochem. J. 141*, 667−673.

(27) Franzen, J. S., Marchetti, P. S., Lockhart, A. H., and Feingold, D. S. (1983) Special effects of UDP-sugar binding to bovine liver uridine diphosphoglucose dehydrogenase. *Biochim. Biophys. Acta 746*, 146−153.

(28) Chen, A., Marchetti, P., Weingarten, M., Franzen, J., and Feingold, D. (1974) Binding studies with bovine liver UDP-D-glucose dehydrogenase. *Carbohydr. Res. 37*, 155−165.

(29) Campbell, R. E., Sala, R. F., van de Rijn, I., and Tanner, M. E. (1997) Properties and kinetic analysis of UDP-glucose dehydrogenase from group A streptococci. Irreversible inhibition by UDP-chloroacetol. *J. Biol. Chem. 272*, 3416−3422.

(30) Ordman, A., and Kirkwood, S. (1977) UDP-glucose dehydrogenase. Kinetics and their mechanistic implications. *Biochim. Biophys. Acta 481*, 25−32.

(31) Zimmerman, S. B., and Trach, S. O. (1991) Estimation of macromolecule concentrations and excluded volume effects for the cytoplasm of *Escherichia coli*. *J. Mol. Biol. 222*, 599−620.

(32) Cayley, S., Lewis, B. A., Guttman, H. J., and Record, M. T., Jr. (1991) Characterization of the cytoplasm of *Escherichia coli* K-12 as a function of external osmolarity. Implications for protein-DNA interactions in vivo. *J. Mol. Biol. 222*, 281−300.

(33) Minton, A. P. (1992) Confinement as a determinant of macromolecular structure and reactivity. *Biophys. J. 63*, 1090−1100.

(34) Kozer, N., and Schreiber, G. (2004) Effect of crowding on protein-protein association rates: Fundamental differences between low and high mass crowding agents. *J. Mol. Biol. 336*, 763−774.

(35) Snoussi, K., and Halle, B. (2005) Protein self-association induced by macromolecular crowding: A quantitative analysis by magnetic relaxation dispersion. *Biophys. J. 88*, 2855−2866.

(36) Franzen, J. S., Marchetti, P., Ishman, R., and Ashcom, J. (1978) Half-sites oxidation of bovine liver uridine diphosphate glucose dehydrogenase. *Biochem. J. 173*, 701−704.

(37) Eccleston, E. D., Thayer, M. L., and Kirkwood, S. (1979) Mechanisms of action of histidinol dehydrogenase and UDP-Glc

dehydrogenase. Evidence that the half-reactions proceed on separate subunits. *J. Biol. Chem. 254*, 11399−11404.
(38) Franzen, J. S., Ashcom, J., Marchetti, P., Cardamone, J. J., Jr., and Feingold, D. S. (1980) Induced versus pre-existing asymmetry models for the half-of-the-sites reactivity effect in bovine liver uridine diphosphoglucose dehydrogenase. *Biochim. Biophys. Acta 614*, 242−255.
(39) Diederichs, K., and Karplus, P. A. (1997) Improved R-factors for diffraction data analysis in macromolecular crystallography. *Nat. Struct. Biol. 4*, 269−275.
(40) Schuck, P. (2000) Size-distribution analysis of macromolecules by sedimentation velocity ultracentrifugation and Lamm equation modeling. *Biophys. J. 78*, 1606−1619.
(41) Laskowski, R. A., and Swindells, M. B. (2011) LigPlot+: Mmultiple ligand-protein interaction diagrams for drug discovery. *J. Chem. Inf. Model. 51*, 2778−2786.